

# An Experimental and Kinetic Modeling Study of Methyl Formate Oxidation

S. Dooley<sup>\*1</sup>, M. Chaos<sup>1</sup>, M.P. Burke<sup>1</sup>, Y. Stein<sup>1</sup>, F.L. Dryer<sup>1</sup>, C.A. Daly<sup>2</sup>, V.P. Zhukov<sup>2</sup>, O. Finch<sup>2</sup>, J.M. Simmie<sup>2</sup> and H.J. Curran<sup>2</sup>

<sup>1</sup>Department of Mechanical and Aerospace Engineering, Princeton University, Princeton, NJ 08544, USA

<sup>2</sup>Combustion Chemistry Centre, National University of Ireland, Galway, Ireland

## Abstract

The combustion of methyl formate ( $\text{CH}_3\text{OCH}(\text{O})$ ) has been studied in three experimental apparatus over a wide range of conditions; a variable pressure flow reactor provides speciation data, shock tubes are used for ignition delay measurements and laminar burning velocities have been measured using outwardly propagating flames.

A detailed chemical kinetic model has been constructed, validated against the wide-ranging experimental data, and employed to interpret the experimental observations. Over most conditions the kinetic model shows a molecular elimination reaction of methyl formate forming methanol and carbon monoxide to of importance.

## Introduction

There has been recent interest in studying various oxygenated fuels for their ability to reduce the emission of  $\text{CO}$ ,  $\text{NO}_x$ , particulates and non-methane hydrocarbons from diesel engines. Dimethyl ether (DME) and dimethoxy methane (DMM) are two of the fuels that have been proposed to either replace totally or be blended with conventional diesel fuel to reduce particulate emissions. Emissions are reduced, apparently, primarily by a reduction in the formation of particulates rather than an increased rate of *insitu* particulate oxidation. By reducing particulate emissions at a certain operating condition, other adjustments in diesel operating parameters (specifically injection timing and exhaust gas recirculation) can be made to reduce  $\text{NO}_x$  emissions. Thus the use of these oxygenated fuels relaxes the typical particulate/ $\text{NO}_x$  trade-off constraints normally found in using conventional diesel fuels. The major intermediate formed in the oxidation of DMM in addition to those found in the oxidation mechanism of DME is methyl formate (MF). Although methyl formate is an intermediate in the oxidation of DME in the presence of  $\text{NO}_x$ , it appears to be only a minor species of little importance in the pure oxidation reaction, particularly at high temperatures. Therefore, the oxidation of MF is of special interest as, in the presence of  $\text{NO}$ , it is a major intermediate in the oxidation of DME as shown by Liu et al. [1].

Secondly, methyl esters of varying alkyl chain length are the primary constituent of biodiesel. For these reasons MF has been the subject of two previous kinetic modeling studies, in 2000 Fisher et al. [2] constructed detailed kinetic models for the oxidation of MF and its n-alkyl cousin, methyl butanoate. However it is was not until very recently that appropriate experimental data was available with which to perform validation. Westbrook et al [3] studied the fuel-rich oxidation of a series of esters in very low pressure ( $\sim 25$  Torr) flames and a submechanism for MF oxidation was able to reproduce the experimental data quite well.

## Specific objectives

MF represents the simplest methyl ester and as such its study allows for the isolation of the role of the ester functionality on combustion processes. In this study we characterize by experiment precise details of MF combustion over a wide range of conditions. By new estimations of the chemical reaction rate and thermochemical parameters involved in MF oxidation we seek to improve upon prior mechanistic work on MF oxidation. As well as refining our understanding of the oxidation mechanism of DMM and DME, these refined parameters may be applied by analogy to larger methyl ester systems such as methyl butanoate and methyl decanoate, as put forth by Dooley [4] and Westbrook et al. [3].

## Experimental

The autoignition of MF was studied at the conditions described in Table 1 using two separate shock tube facilities at NUI, Galway. The  $\sim 2.7$  atm data were gathered using a low pressure instrumented shock tube.

Mix	$\Phi$	MF	$\text{O}_2$	Ar	T/K	p/atm
1	2.0	0.5	0.5	99.0	1285–1935	2.7
2	1.0	0.5	1.0	98.5	1275–1780	2.7
3	0.5	0.5	2.0	97.5	1420–1690	5.4
4	1.0	2.5	5.0	92.5	1130–1660	9.4

Table 1: Conditions of shock tube study.

The higher pressure  $\sim 5.4$  and  $\sim 9.4$  atm data were obtained with a new high pressure shock tube facility constructed at NUI, Galway. Both shock tubes were used to study MF autoignition under reflected shock conditions, the essential difference between the two instruments being the method of incident shock wave generation.

## Low pressure shock tube

The low pressure shock tube has been described thoroughly elsewhere [5]. This apparatus has been used to study the auto ignition of mixtures (1) and (2) at

\* Corresponding author: [dooleys@princeton.edu](mailto:dooleys@princeton.edu)

reflected shock pressures of  $2.7 \pm 0.3$  atm and reflected shock temperatures of 1275–1935 K, Table 1.

#### High pressure shock tube

The high pressure shock tube facility existed in a previous incarnation in the laboratory of Prof. Cadman [6] and maintains essentially the same parameters of operation and performance. Re-commissioned in 2007 this shock tube consists of an 876 cm stainless steel tube of internal diameter 63 mm, divided into a 300 cm long driver section and a test section 573 cm in length. The high pressure drive section is further divided for the generation of shock waves by the double diaphragm rupturing technique. Polycarbonate diaphragms separate a small chamber containing helium drive gas at intermediate pressure from the high pressure drive section and the low pressure test section. The sudden evacuation of this intermediate pressure causes both diaphragms to rupture allowing incident shock waves to form in a reproducible manner. This apparatus was used to generate higher pressure reflected shock waves of  $5.4 \pm 0.4$  atm and  $9.4 \pm 0.4$  atm for the study of mixtures (3) and (4) respectively, Table 1.

Similarly to the low pressure shock tube arrangement, three pressure transducers (PCB 113A24) were set into the final 50 cm of the test section and a fourth is embedded in the end wall. In conjunction with three time counters (Fluke PM6666) these pressure sensors allow for the measurement of the incident shock velocity at three points as the shock wave passes along the test section. Reflected shock conditions were calculated using one-dimensional shock relations as implemented by the application GasEq [7]. The estimated error in the measurement of incident shock velocity corresponds to an uncertainty in reflected shock temperature of  $\pm 7$  K, such is represented by error bars in Figs. 3 & 4 [8].

In both apparatus helium CP Grade 99.999%, was used as drive gas. Test gas mixtures for study in both instruments were prepared in 50 L stainless steel tanks using standard manometric methods, argon was Zero Grade 99.998%, and oxygen was Research Grade 99.985%. All gases were obtained from BOC Ireland Ltd and used without further purification. Methyl formate as 99.5% pure was obtained from Aldrich Chemical Co. Ltd. To minimize the presence of atmospheric air in the liquid fuel the sample was subjected to several freeze-pump-thaw degassing cycles before being incorporated into the test mixture by vaporization into the evacuated mixing tanks. The high pressure shock tube facility uses a Wallace and Tiernan (61b-1a-0050e) 0–3400 mbar pressure gauge to measure fuel, oxygen and diluent partial pressures. Test gas mixtures were normally made up to a final pressure of 800 Torr and allowed to stand for at least 12 hours to ensure homogeneity.

Light emission was observed in each experiment with the use of a 431.5 nm narrow bandpass filter with a spectral bandwidth of 10 nm. The filters and the light diagnostics were aligned behind quartz windows located

in each end wall. The pressure transducers, mounted flush with each end wall, signaled the shock wave arrival at the end wall and the beginning of the ignition delay period. The end of the period was defined as the maximum rate of CH\* emission.

#### Variable Pressure Flow Reactor (VPFR)

The design and operating characteristics of the Princeton VPFR have been discussed in detail elsewhere [9–11]. In the present experiments, nitrogen carrier gas was heated by an electric resistance heater and mixed with oxygen as it entered a 10.2-cm-diameter quartz test section. MF (99.5%, Aldrich Chemical Co. Ltd.) was supplied from a liquid evaporator system, diluted with additional nitrogen. The diluted fuel vapor was rapidly mixed with the carrier gas at the entrance to a conical shaped silica foam diffuser. The reaction temperature of flow at the sampling location, with all flows established except the fuel flow, varied by less than  $\sim 2$  K. During operation of the VPFR, all flow rates of carrier, diluent, and reactants were metered and held constant for the entire duration of each set of experiments reported. The initial reaction temperature not accounting for combustive heat release was held constant. Throughout the course of each experiment the reaction pressure was modified so as to maintain the initial reaction pressure. The reaction temperature at the sampling location and all sample analytical readings were allowed to achieve steady state, before the data were digitally recorded.

The reaction (residence) time was varied by changing the distance between the fuel injection location and the fixed sampling probe. The sampled gas flow was transferred through heated Teflon lines to a series of analytical equipment including a Fourier transform infrared (FTIR) spectrometer (Nicolet Model 560), an electrochemical oxygen ( $O_2$ ) analyzer (Infrared Industries Model 2200), and non-dispersive carbon monoxide (CO) and carbon dioxide ( $CO_2$ ) analyzers (Horiba Model PIR 2000). The uncertainties in the measurements reported here are:  $O_2 < 4\%$ ;  $CO < 3\%$ ;  $CO_2 < 3\%$  of the reading. The other major species identified during the oxidation of MF were  $H_2O$  (water),  $CH_3OH$  (methanol),  $CH_2O$  (formaldehyde) and  $CH_4$  (methane). These species were quantified by online FTIR spectroscopy, estimated uncertainties in these measurements are:  $H_2O < 5\%$ ;  $MF < 3\%$ ;  $CH_3OH < 3\%$ ;  $CH_2O \sim 10\%$ ;  $CH_4 < 3\%$  of the reported value.

Set	$\Phi$	MF	$O_2$	$N_2$	T/K	p/atm
1	0.5	0.5	2.0	97.5	900	3.0
2	1.0	0.5	1.0	98.5	903	3.0
3	1.5	0.5	0.67	98.8	900	3.0

Table 2: Conditions of VPFR study

The oxidation of MF was studied using 0.5% fuel, at three equivalence ratios ( $\Phi$ ): 0.5, 1.0 and 1.5. Pressure was held constant at 3 atm and initial reactor temperatures were  $\sim 900$  K, Table 2. The reaction was followed as a function of time until the fuel and major intermediates had been consumed,  $\sim 0.7$  seconds.

### Dual chambered cylindrical bomb

The burning velocities of MF/O<sub>2</sub>/N<sub>2</sub> flames were measured as a function  $\Phi$  using outwardly propagating flames in a dual-chambered, pressure-release type high-pressure combustion apparatus as described in detail elsewhere [12]. In the present study, the device was operated in the “closed” configuration, and may be treated as a constant-volume cylindrical bomb. Mixtures were prepared in the constant volume chamber by the partial pressure method using an absolute pressure gauge (Cecomp Electronics Inc.) of 0.25% full scale accuracy. For all experiments methyl formate (anhydrous, 99%, Aldrich Chemical Co. Ltd.) was diluted to a pressure of 1 atm with synthetic air, i.e. O<sub>2</sub>:N<sub>2</sub> = 1:3.78, consisting of Zero Grade nitrogen (99.998%) and Research Grade oxygen (99.5%) supplied by Airgas Ltd. Due care was taken to ensure that there was minimal contamination of the methyl formate vapor in filling the combustion chamber. The mixtures were allowed to homogenise for 30 minutes prior to spark induced ignition by a high voltage tungsten filament. The initial temperature of each experiment was 295±2K.

The flame radius was recorded from Schlieren images obtain with a high speed video camera as a function of time. The instantaneous flame speed ( $s_u$ ) is calculated using a flow correction term ( $\varpi$ ) [13]. The flow correction term is employed to account for the actual gas motions induced by combustion, rather than the conventional zero burned gas velocity assumption ( $\varpi = 0$ ). The expansion factor ( $\sigma$ ) is defined as the ratio of the unburned to burned gas densities across the flame front.

$$s_u = \frac{\frac{1}{\sigma} \frac{dr_f}{dt}}{\left(1 + \frac{\sigma - 1}{\sigma} \varpi\right)}$$

The definition of stretch rate ( $\kappa$ ) is that of Strehlow and Savage [14] and may be related to the flame radius ( $r_f$ ) and flame front velocity ( $dr_f/dt$ ) by,

$$\kappa = \frac{2}{r_f} \frac{dr_f}{dt}$$

The laminar burning velocity ( $s_u^o$ ), is obtained through linear extrapolation of the flame speed to a value of zero stretch rate using a linear stretch relation,

$$s_u = s_u^o - L_u \cdot \kappa$$

where  $L_u$  is the Markstein length. Prolonged unsteady ignition effects were observed up to flame radii of 1 cm for some conditions. Therefore, linear extrapolation to the laminar burning velocity is performed for flame radii ranging from 1 to 2 cm where the quasi steady linear stretch relationship appears more valid. This methodology was tested by extrapolating to zero stretch rate over four distinct ranges of flame radii (from 1 to 3cm) for each experiment. This treatment produced burning velocities which were typically consistent

within 3% (the value of the error bars presented in Fig. 5). Four experiments were conducted at the stoichiometric condition, where mixing time was varied from 30 to 115 minutes. The burning velocity for each case is consistent within 2%. All other values presented are obtained from single experiments.

### Computational Simulations

The modeling computations in this study were carried out using the Chemkin suite of programs (*SENKIN* and *PREMIX*) [15]. Shock tube simulations assume constant volume adiabatic conditions behind the reflected shock wave and we define the simulated ignition delay time as in [8].

The VPFR experiments may be modeled as a zero-dimensional system with isobaric and adiabatic approximations [10]. In the present experiments MF is observed to be converted to methanol and carbon monoxide at the earliest residence times observed. For example, the stoichiometric condition shows ~30% of the fuel to be converted directly to CH<sub>3</sub>OH + CO at a residence time of only 0.02 seconds, with only trace oxidation products observed, Fig. 2(t). The inlet conical diffuser is composed of fused silica. Considering the establishing literature [8] regarding the problematic use of this material in controlled oxidation experiments for oxygenated fuels, we take the high levels of CH<sub>3</sub>OH + CO at residence times corresponding to sampling distances inside the diffuser to be evidence of the wall catalysed (heterogeneous) unimolecular decomposition of fuel. These effects have been shown to be negligible in the constant diameter quartz test section [10]. However in order to compare this data to the predictions of a kinetic model one must account for the change in mixture composition due to the non-gaseous effects inside the mixer/diffuser section of the VPFR. This is accomplished by employing the technique of initialization as described by Zhao et al. [10]. The species output from this simulation is input to *SENKIN* and the simulation is continued under isobaric and adiabatic assumptions.

The laminar burning velocities were calculated by simulating freely propagating flames using the *PREMIX* module considering multicomponent transport and thermal diffusive effects. Simulations were performed over a constant domain size ranging from -5cm to 5cm. The use of one thousand grid points assures that stringent increments of 0.01 for both *CURV* and *GRAD* may be met and that the reported solutions are independent of grid size. All Figures in this study depict experimental measurement as symbols and kinetic modeling simulation as lines.

### Chemical Kinetic Model

A detailed chemical kinetic model for methyl formate oxidation has been constructed and used to simulate this experimental data. No low temperature reactivity has been reported for MF and so we have not include the reaction of  $\cdot R + O_2 \rightarrow \cdot RO_2$  and subsequent reactions of the  $\cdot RO_2$  species. This chemistry may be

added to the present high temperature mechanism should it be required. As the molecular structure of methyl formate is void of C–C bonds we expect the formation of any C<sub>2</sub> species during MF oxidation to be minimal. Indeed no C<sub>2</sub> intermediate species were observed in our VPFR experiments. However we do allow this chemistry to occur. The MF chemistry is added to a submechanism consisting of the C<sub>1</sub> mechanism of Li et al. [16] and the C<sub>4</sub> chemistry of Bourque et al. [17]. This particular set of base chemistry was chosen for its accuracy in describing the oxidation of methanol, a primary intermediate species in MF oxidation.

The thermochemical parameters of oxygenated species are not as well known as those of conventional hydrocarbon fuels. Hall and Baldt [18] have measured by bomb calorimetry H<sub>f</sub><sup>o</sup><sub>298 K</sub> of MF as -84.97 kcal mol<sup>-1</sup>. There are non-experimental values in the literature which describe the influence of the ester functionality on any surrounding atoms; Good and Francisco [19] Glaude et al. [20] and Sumanthi and Green [21] have all computed by different quantum chemical methods the H<sub>f</sub><sup>o</sup><sub>298 K</sub> for MF as well as several species formed by its oxidation. The C–H bond dissociation enthalpies (BDE) which result from this data are shown in Table 3.

Bond	Good <sup>[19]</sup>	Glaude <sup>[20]</sup>	Sumanthi <sup>[21]</sup>
CH <sub>3</sub> OC(O)–H	100.3	100.3	100.1
H–CH <sub>2</sub> OCH(O)	101.3	101.9	100.9
MF H <sub>f</sub> <sup>o</sup> <sub>298 K</sub>	-85.7	-86.0	-85.9

Table 3: MF thermochemical data at 298 K /kcal mol<sup>-1</sup>

All values for the CH<sub>3</sub>OC(O)–H BDE are in excellent agreement, but the reported values for the H–CH<sub>2</sub>OCH(O) BDE differ by ~1 kcal mol<sup>-1</sup>. Therefore our treatment of hydrogen abstraction from this site is a source of error in the kinetic model. We have chosen to generate the thermochemical input for the kinetic model with use of the group values recommended by Sumanthi and Green. We implement these values by the method of group additivity [22] as employed through THERM [8] and arrive at a set of BDEs as shown in Fig. 1. Hydrogen abstraction from MF may occur from two locations producing the radical species CH<sub>3</sub>O·C(O) and ·CH<sub>2</sub>OCH(O). Oxygenated fuels can exhibit unorthodox C–H BDEs, particularly if these bonds are in close proximity to the electronegative oxygen atoms.

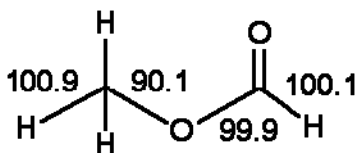


Figure 1: MF bond enthalpies at 298K / kcal mol<sup>-1</sup>

As most of the available rate data deals with conventional hydrocarbon fuels, this facet of the detailed modeling of oxygenates represents a significant challenge. It is our intention to develop a deductive *a priori* approach to the estimation of the rate of hydrogen abstraction from such systems. We assume that the rate

of abstraction is dependent on the identity of the abstracting radical and on the strength of the C–H bond. With the use of extensively reviewed literature data [18] on hydrogen abstraction from regular hydrocarbons (such as propane and ethane) the rate of hydrogen abstraction may be correlated with the BDE on a per H atom basis for C–H BDEs of 100.1 and 100.9 kcal mol<sup>-1</sup> respectively. This method allows the sensitivity to the rate of hydrogen abstraction to be confidently tested within the known uncertainties of the thermochemical parameters.

MF may decompose by homolysis of C–H and C–O bonds. The high-pressure limit rate expressions for these reactions have been estimated in the reverse recombination direction, which is taken to be a barrierless process. The forward decomposition expression is computed from microscopic reversibility and in this manner the BDE is taken into account.

MF may also decompose through a number of concerted molecular elimination reactions. We consider two channels; MF → CH<sub>3</sub>OH + CO and MF → CH<sub>4</sub> + CO<sub>2</sub>. Although Francisco [23], using six levels of theory, calculated the energy barrier of the transition state which leads to the formation of CH<sub>3</sub>OH + CO to be 74–77 kcal mol<sup>-1</sup>, the overall rate of this three-centered reaction is not known. In the present study we have taken it to equal that of the four-centered molecular elimination reaction of methyl tert-butyl ether (MTBE) forming isobutene and methanol. This reaction has been studied by experiment four times and a NIST kinetic database [18] fit yields a rate expression of 1.00 × 10<sup>14</sup> exp (-60,000 cal mol<sup>-1</sup>/RT) cm<sup>3</sup> mol<sup>-1</sup> s<sup>-1</sup>. We prefer this analogy as reasonable as the ring strain values for three and four membered transition states are recommended by Benson [22] to be 26.9 and 25.7 kcal mol<sup>-1</sup>, respectively. In addition, the frequency factors for these reactions ought to be similar. The MF transition state has one less rotor available to it than that for MTBE, and so should be almost an order of magnitude faster. However, MTBE has nine hydrogen atoms available for the hydrogen transfer, compared to only one in the case of MF, and so the A-factors should be very similar.

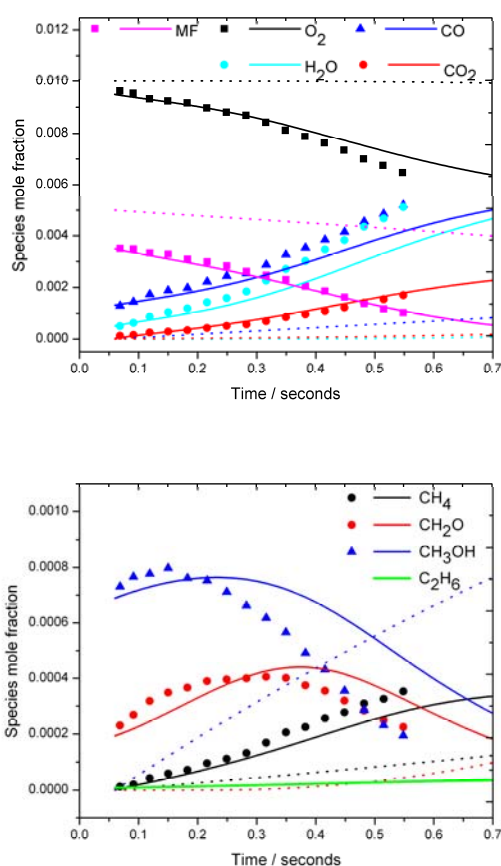
Recognizing that the branching ratio between MF decomposing to CH<sub>3</sub>OH + CO and CH<sub>4</sub> + CO<sub>2</sub> is likely as important as the absolute value of the rate constants, we have estimated our rate expression for the latter channel in consistent fashion with our estimate of the former. In this regard the transition state leading to CH<sub>4</sub> + CO<sub>2</sub> is four centered and therefore eliminates one more rotor than the three-centred reaction. This ought to lower the frequency factor by almost an order of magnitude, while the activation energy should be only slightly lower. We estimate a rate expression for the reaction MF → CH<sub>4</sub> + CO<sub>2</sub> of 8.00 × 10<sup>12</sup> exp (-59,000 cal mol<sup>-1</sup>/RT) cm<sup>3</sup> mol<sup>-1</sup> s<sup>-1</sup>. In this instance we apparently disagree with the calculations of Francisco [26], who has computed the barrier to formation of CH<sub>4</sub> + CO<sub>2</sub> to be higher than that for CH<sub>3</sub>OH + CO formation, lying at ~85 kcal mol<sup>-1</sup>. The resultant rate

constants for these elimination reactions and that of  $\text{MF} \rightarrow \cdot\text{CH}_3 + \cdot\text{OCH}(\text{O})$  have also been treated using quantum Rice-Ramsperger-Kassel theory with a master equation analysis [8] in order to account for pressure fall-off.

In order to simulate the burning velocity data transport parameters for species of the MF sub mechanism have been estimated based on those of dimethyl ether, which is of similar molecular mass.

## Results and Discussion

Figs. 2(t) and 2(b) show speciation data measured during the oxidation of MF at 3 atm and  $\sim 900$  K in the VPFR for the  $\Phi = 1.0$  condition versus model agreement. Though not shown here the model performs similarly against the  $\Phi = 0.5$  and  $\Phi = 1.5$  conditions.



Figures 2(t/top) & (b/bottom): Flow reactor data for 0.5/1.0/98.5 MF/O<sub>2</sub>/N<sub>2</sub>,  $\Phi = 1.0$  at 3.0 atm & 905 K

As discussed, over all conditions high levels of methanol and carbon monoxide are present very early in reaction. In simulation this effect is accounted for by the described initializing technique [10]. The dotted lines in Fig. 2 show model agreement assuming no catalytic wall effect occurs. The data shows substantial levels of methane to be produced during the combustion of MF, yet no C<sub>2</sub> species were observed in experiment. This is interesting as it indicates that methyl radicals do not play a significant role in MF oxidation under these conditions. If methane were being formed by methyl

radical hydrogen abstraction from fuel or by the reaction  $\cdot\text{CH}_3 + \text{H}\cdot\text{O}_2 \rightarrow \text{CH}_4 + \text{O}_2$  as in other systems, one would expect the reaction  $\cdot\text{CH}_3 + \cdot\text{CH}_3 \rightarrow \text{C}_2\text{H}_6$  to yield measurable ethane concentrations. The simulated ethane profile is included in Fig. 2(b). Indeed both experiment and model show that methane is most substantially formed by molecular elimination from MF with a smaller contribution from  $\cdot\text{CH}_3$  radical recombination with the abundant H $\cdot$ O<sub>2</sub> radical. Until a residence time of  $\sim 0.2$  seconds the major channel consuming the fuel is the reaction of  $\text{MF} \rightarrow \text{CH}_3\text{OH} + \text{CO}$ , however after this time the radical pool becomes established and hydrogen abstraction from fuel by  $\cdot\text{H}$  atom and  $\cdot\text{OH}$  radical become the dominant fuel consumption pathways. CH<sub>2</sub>O is formed by the consumption of CH<sub>3</sub>OH, with only a small contribution from the decomposition of the fuel radical,  $\cdot\text{CH}_2\text{OCH}(\text{O})$ .

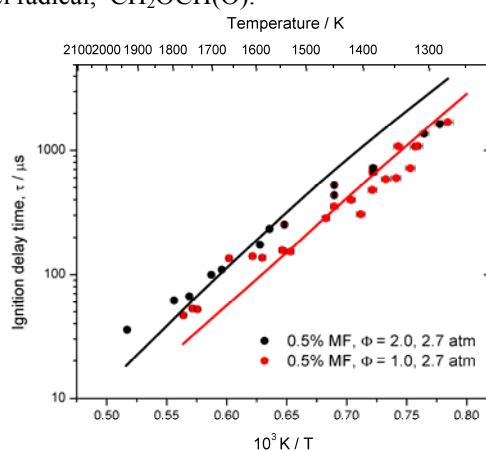


Figure 3: Shock tube ignition delay times for MF/O<sub>2</sub>/Ar mixtures (1) and (2) at pressures of 2.7 ± 0.3 atm

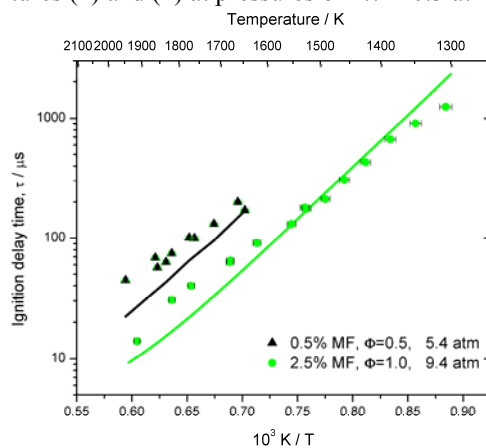


Figure 4: Shock tube ignition delay times for MF/O<sub>2</sub>/Ar mixtures (3) and (4) at pressures of 5.4 and 9.4 ± 0.4 atm

The performance of the kinetic model against shock tube ignition data is presented in Figs. 3 & 4. Each set of ignition delays show Arrhenius temperature dependence. At 2.7 atm, the experimental data in Fig. 3 show only a slight effect of O<sub>2</sub> concentration at constant fuel concentration. The kinetic model does reproduce this effect but shows a stronger dependency on O<sub>2</sub> concentration than observed in experiment. The weak

dependency on  $O_2$  concentration observed in experiment is interesting as it indicates a departure from traditional high temperature oxidation kinetics observed for hydrocarbons and oxygenates, where the rate of the chain branching reaction,  $\cdot H + O_2 \rightarrow \cdot O + \cdot OH$  dominates the reactivity. The kinetic model shows that almost all MF in the system decomposes very early in reaction to form  $CH_3OH + CO$  with  $< 5\%$  of the fuel consumed by hydrogen abstraction reactions.

Although mixtures 3 and 4 are significantly different their ignition delays are plotted together in Fig. 4. The kinetic model is able to reproduce this data with reasonable accuracy, although the higher temperature ignition delays for the 5.4 atm case are under predicted by almost a factor of two. In general the kinetic model is correct in its prediction of the ignition data but further effort is required to reconcile more precisely discrepancies between experiment and model.

The laminar burning velocity ( $s_u^o$ ) at 1 atm of MF/ $O_2/N_2$  mixtures is compared to model predictions as a function of equivalence ratio in Fig. 5. Experiment shows that the value of  $s_u^o$  varies as a function of equivalence ratio from low values of  $\sim 24 \text{ cm s}^{-1}$  at  $\Phi=0.8$  and  $\Phi=1.6$ , to a peak value of  $37.5 \text{ cm s}^{-1}$ . This general dependency of  $s_u^o$  on equivalence ratio, with a peak to the fuel rich side of stoichiometric is similar to that seen for the burning velocities of hydrocarbons and the relatively fewer published measurements of oxygenates. The model reproduces this data well, though to be particular, predictions of  $s_u^o$  for the fuel leaner mixtures ( $\Phi = 0.8-1.1$ ) are consistently fast. In general although the shock tube ignition data and this flame data share a common temperature regime of  $\sim 1000-2000 \text{ K}$ , the specifics of the chemistry of fuel consumption are different. While in the shock tube the model shows MF to be immediately consumed by the reaction of  $MF \rightarrow CH_3OH + CO$ , the radical rich nature of a flame allows MF to be exclusively consumed by hydrogen abstraction reactions (by  $\cdot O$ ,  $\cdot H$  and  $\cdot OH$  radicals) until temperatures above  $\sim 1400 \text{ K}$ .

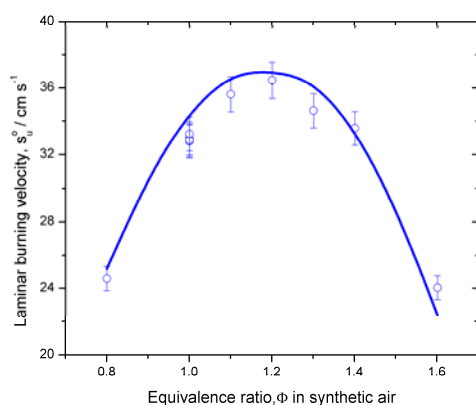


Figure 5: Burning velocities for MF/ $O_2/N_2$  mixtures.

## Conclusions

The mechanism of methyl formate combustion is shown to proceed to a large extent through the molecular

elimination;  $MF \rightarrow CH_3OH + CO$ . Due to this effect we observe only a weak dependence of ignition delay time on  $O_2$  concentration.

## Acknowledgements

Work at Princeton University was supported by the U.S. Department of Energy by Grant No. DE-FG02-86ER13503 from the Office of Basic Energy Sciences.

## References

- [1] I. Liu, N.W. Cant, J.H. Bromly, F.J. Barnes, P.F. Nelson and B.S. Haynes, *Chemosphere* 42 (2001) 583–589.
- [2] E.M. Fisher, W.J. Pitz, H.J. Curran, C.K. Westbrook, *Proc. Combust. Inst.* 28 (2000) 1579–1586.
- [3] C.K. Westbrook et al., *Proc. Combust. Inst.* 32 (2009) 221–228.
- [4] S. Dooley, Ph.D. Thesis 2008 National University of Ireland, Galway.
- [5] J.M. Smith, J.M. Simmie, H.J. Curran, *Int. J. Chem. Kinet.* 37 (2005) 728–736.
- [6] P. Cadman, G.O. Thomas, P. Butler, *Phys. Chem. Chem. Phys.* 2 (2000) 5411–5419.
- [7] C. Morley, <http://www.gaseq.co.uk/>
- [8] S. Dooley, H.J. Curran, J.M. Simmie, *Combust. Flame* 153 (2008) 1–52.
- [9] T.J. Held, F.L. Dryer, *Int. J. Chem. Kinet.* 30 (1998) 805–830.
- [10] Z. Zhao, M. Chaos, A. Kazakov, F.L. Dryer, *Int. J. Chem. Kinet.* 10 (2008) 1–18.
- [11] J. Li, Z. Zhao, A. Kazakov, M. Chaos, F.L. Dryer, *Int. J. Chem. Kinet.* 36 (2004) 566–575.
- [12] X. Qin, Y. Ju, *Proc. Combust. Inst.* 30 (2005) 233–240.
- [13] M.P. Burke, Z. Chen, Y. Ju, F.L. Dryer, *accepted to Combust. Flame* (2009).
- [14] R.A. Strehlow, L.D. Savage, *Combustion and Flame* 31 (1978) 209–211.
- [15] R.J. Kee et al., *Chemkin Collection*, Release 3.6, Reaction Design, Inc., 2000.
- [16] J. Li, Z. Zhao, A. Kazakov, M. Chaos, F.L. Dryer, J.J. Scire, Jr., *Int. J. Chem. Kinet.* 39 (2007) 109–136.
- [17] G. Bourque et al. *submitted to J. Eng. Gas Turb. Power*, 2007.
- [18] NIST Chemical Kinetics Database 17, Version 7.0, Release 1.4.2, Data Version 2009.0.
- [19] D.A. Good, J.S. Francisco, *J. Phys. Chem. A.* 104 (2000) 1171–1185.
- [20] P.A. Glaude, W.J. Pitz, M.J. Thomson, *Proc. Combust. Inst.* 30 (2005) 1111–1118.
- [21] R. Sumanthi, W.H. Green Jr., *Phys. Chem. Chem. Phys.* 5 (2003) 3402–3417.
- [22] S.W. Benson in: *Thermochemical Kinetics*, 1976, John Wiley and Sons, Inc., New York.
- [23] J.S. Francisco, *J. Am. Chem. Soc.* 125 (2003) 10475–10480.